Optical Materials 138 (2023) 113684

Contents lists available at ScienceDirect

Optical Materials

journal homepage: www.elsevier.com/locate/optmat

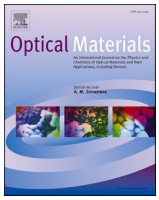

Research Article

Structure-dependent optical properties of Au/Ag irradiated TiN thin films

M. Popović [a,*], M. Novaković [a], D. Vaňa [b], C. Ronning [c], D. Jugović [d], V. Rajić [a], P. Noga [b]

[a] Department of Atomic Physics, Vinča Institute of Nuclear Sciences - National Institute of The Republic of Serbia, University of Belgrade, Belgrade, Serbia
[b] Slovak University of Technology in Bratislava, Faculty of Materials Science and Technology in Trnava, Advanced Technologies Research Institute, Trnava, Slovakia
[c] Institute of Solid State Physics, Friedrich Schiller University Jena, Max-Wien-Platz 1, D-07743, Jena, Germany
[d] Institute of Technical Sciences of SASA, Belgrade, Serbia

ARTICLE INFO

Keywords:
Titanium-nitride
Silver
Gold
Sequential implantation
Structural properties
Optical losses

ABSTRACT

Titanium nitride (TiN) is an attractive alternative for modern and future photonic applications, as its optical properties can be engineered over a wide spectral range. In this study, we have used sequential implantation of gold and silver ions with varying ion fluence, as well as subsequent annealing, in order to modify the optical and plasmonic properties of TiN thin films and correlated this to their structural properties. Our investigations show that the columnar structure of the TiN films is partially destroyed upon implantation, but metallic Au and Ag nanoparticles are formed. The irradiation further induces a reduction of the lattice constant as well as changes the TiN stoichiometry and grain size. From the optical point of view, the implanted films possess less metallicity with increasing Ag fluence and losses several times lower than the as-deposited film, which can be correlated with the deficiency of nitrogen and additional defects. Subsequent annealing partially recovered the destroyed columnar structure, and the films become more metallic where the optical losses are much smaller in comparison to the as-implanted situation, being comparable to those of pure Au and Ag. In this way, by varying the implantation fluence of silver ions properly while keeping the gold fluence constant, we were able to optimize experimental parameters in such a way to ensure the formation of TiN with desirable optical performances.

1. Introduction

Transition metal nitrides possessing an admixture of the properties of covalent compounds, ionic crystals, and transition metals, have attracted tremendous research interest over the past decades. Their unique electronic structure, high electrical conductivity, high melting point, superior mechanical stability, chemical inertness and compatibility with a wide number of substrate materials made them technologically very important [1–3]. Specifically, one of advantages of transition metal nitrides is their compatibility with complementary metal-oxide-semiconductor (CMOS) technology, enabling besides the lower fabrication costs also easy integration and upscaling in mainstream industrial electronic devices without the concern of volume expansion and stress at the interface due to diffusion [4,5]. Demonstrating many of these advantages, titanium nitride (TiN) is probably the most investigated transition metal nitride readily used by the industry, mainly as a protective [6] or decorative coating [7], but also in microelectronics acting as an efficient anti-diffusion layer [8], adhesion layer [9], and top-gate in field-effect transistors [10]. Another field of application is in plasmonics, where TiN became an attractive alternative for modern and future photonic applications due to its high Drude like reflectance in the IR spectrum and high absorption in the visible and near-IR region, successfully replacing and, in some areas, overcoming gold [11–15]. Thus, TiN offers fabrication and integration advantages that could be useful in integrating plasmonics with nanoelectronics.

Up to now, titanium nitride has been studied extensively in terms of adjustable properties with varying fabrication methods and parameters depending on the application area [16–25]. For example, Patsalas et al. [26,27] found that the optical, electrical and transport properties as well as hardness and elastic modulus of TiN can be tailored by varying the substrate temperature and the energy of bombarding ions during sputter deposition, showing that both parameters determine the stoichiometry and microstructural features of the nanocrystalline films. Further, Liang et al. [28] have shown that by changing the deposition time, the roughness, crystallite size, density and resistivity of the TiN films can be successfully controlled making titanium-nitride suitable as a metal gate and capacitor electrode in microelectronic devices. As for the optical performances of TiN, many studies have been reported with the main effort to optimize the permittivity and most importantly to reduce the optical losses to less than that of noble metals in a broad spectral range

* Corresponding author. Institute of Nuclear Sciences VINČA, Mike Petrovića Alasa 12-14, 11 000, Belgrade, Serbia.
E-mail address: majap@vinca.rs (M. Popović).

https://doi.org/10.1016/j.optmat.2023.113684
Received 9 January 2023; Received in revised form 3 March 2023; Accepted 9 March 2023
Available online 16 March 2023

[29–35]. Apart from the conventional methods for optimizing the performances of the material, an effective way is to change the properties by introducing a certain amount of dopants using ion implantation [36–43]. Besides the possible formation of nanoparticles, which depends on the irradiation conditions, ion implantation is accompanied by defect formation when lattice disorder is produced and consequently the optical and electrical properties are changed.

In our earlier studies [44–46], we have shown that introducing a new element in TiN thin films by ion implantation strongly affects the crystalline structure reducing the lattice size and forming smaller crystallites and/or clusters as well as different types of crystal imperfections. On the other hand, annealing treatments after irradiation reduce the defect concentration and enhances sub-grain growth [47], improving the crystallinity and recovering damage formed during ion implantation. Besides the structural changes, it was found that the optical properties are greatly altered after ion irradiation, which is presented through our comprehensive study of the optical properties of TiN films implanted with silver and gold presented in Refs. [48,49]. Namely, we have found that the implanted films possess optical losses several times lower in comparison to the initial TiN film and is nearly comparable to pure gold. In the present work, we have now investigated in detail the correlation between the microstructural changes induced by sequential Au/Ag ion implantation and post-irradiation annealing, affecting the stoichiometry and microstructure of the TiN films and their optical properties. We address the optical properties of the implanted TiN films in terms of their complex dielectric function measured by spectroscopic ellipsometry while the film's microstructure including the crystal structure, lattice size, crystallite size and stoichiometry were analyzed by X-ray diffraction (XRD) and transmission electron microscopy (TEM).

2. Experiment

Titanium nitride thin films with thicknesses of about 260 nm were prepared on Si substrates by DC reactive sputtering (Balzers Sputtron). A pure Ti target (99.9%) was sputtered in a nitrogen-argon ambient with partial pressures of 1×10^{-1} Pa and 3×10^{-2} Pa of Ar and N_2, respectively. The base pressure in the chamber was 1×10^{-4} Pa. The silicon substrates were single side polished, 550 μm thick, (100) oriented and cleaned by standard procedures; rinsed in dilute HF acid and deionized water as well as sputter-cleaned with a 1.5 keV argon ion beam prior to TiN deposition. Homogenous and polycrystalline TiN films with nearly 1:1 stoichiometry were produced in this way, as already reported in our previous studies [46,50].

The deposited TiN films were ion implanted sequentially with both gold and silver [51]. The first implantation with gold ions was performed for all samples using an ion energy of 200 keV and an ion fluence of 1×10^{16} ions/cm^2. The second implantation with silver ions was done with an ion energy of 150 keV but varying ion fluences of 4×10^{16} ions/cm^2, 7×10^{16} ions/cm^2 and 13×10^{16} ions/cm^2. The values of the ion energies were chosen in such a way that the ion distributions of both species were overlapping. According to SRIM2010 calculations [52] the mean projected range of the incident ions was estimated to be $R_P = 36 \pm 9$ nm and $R_P = 38 \pm 14$ nm for both 200 keV gold and 150 keV silver. The implantation area was homogeneously covered by means of an *x*–*y* sweeping system; the average beam current was kept around 0.22 μA/cm^2 for Au and 0.67 μA/cm^2 for Ag ions. Subsequent to the implantation process, the samples were annealed for 1 h at 500 °C in a furnace, under vacuum in a low 10^{-4} Pa region.

Electron-transparent cross-sectional lamellae were prepared using a focused ion beam (FIB) system (FEI Scios 2 Dual Beam), and subsequent TEM investigations on those lamellae were done by a FEI Talos F200X microscope operating at 200 kV. Besides conventional TEM imaging, high-resolution (HRTEM) and selected area electron diffraction (SAED) studies were carried out in order to obtain additional insights into the nanostructure of the films. In addition, energy dispersive X-ray spectroscopy measurements (EDS) of the samples were performed and used for quantitative analysis characterization. XRD data were collected with a Philips PW1050 diffractometer using $CuK_{\alpha 1,2}$ radiation (Ni filter) at room temperature in Bragg-Brentano geometry. The measurements were done in a 2θ range of 34-45° with a scanning step width of 0.05° and a counting time of 6 s per step. The microstructural parameters, namely the crystallite size (coherently scattering domain) and the microstrain were calculated based on the Fundamental Parameters convolution approach to generate line profile by using XFIT computing program [53]. The optical properties of TiN samples were measured by spectroscopic ellipsometry using a Jobin-Yvon UVISEL spectrometer operated in the wavelength region from 260 nm to 2066 nm (energy range 0.6 eV to 4.8 eV), with a step of 0.1 eV. The spectra were taken in reflection mode, at an angle of incidence of 70° and with spot diameter of 1 mm. The measured data were analyzed using the DeltaPsi2 software [54].

3. Results and discussion

3.1. Microstructure and composition of the films

For detailed information on the microstructural evolution of TiN films, that involves changes induced by the dual Au/Ag ion implantation and subsequent thermal treatment, the samples were analyzed by transmission electron microscopy. Respective results of TEM imaging, experimental SAED patterning, EDS measurements, and HRTEM analysis are summarized in Figs. 1 and 2. Low-magnification TEM bright-field images of the as-deposited TiN layer and the Au/Ag implanted samples (Fig. 1) reveals the general microstructure of the layers before and after implantation. Based on the image contrast one can easily identify ~260 nm thick TiN films between the Si substrates and Pt overlayers, which were deposited as protective layer during FIB preparation of the TEM lamellae. The deposited TiN film has a columnar structure, where the columns diameter of around 10 nm are homogenously distributed across the sample and propagates along the layer. Corresponding electron diffraction pattern, given in the respective insets of Fig. 1, were taken from the selected area of the sample, thus avoiding the presence of highly oriented spots from the crystalline Si substrate. For the as-grown TiN sample in Fig. 1(a), one clearly observes well-defined diffraction rings typical for a fine-grained structure consisting of very small crystals randomly distributed with no preferred orientation. From the radii of the rings, we have calculated d-spacings and determined a value of 0.244 nm for the most inner ring, whereas two outer ones correspond to 0.211 nm and 0.149 nm. The calculated d-spacings exactly match the distances of (111), (200) and (220) planes of face-centered cubic (fcc) TiN lattice, thus confirming that pure TiN was formed during the deposition process.

After Au/Ag implantations the columnar structure was found to be damaged within approximately 100 nm thick top layer at the sample surface, as shown in Fig. 1(b–d) with increasing Ag fluence. The observed change in the microstructure is a result of ion-induced damage that happens during the implantation [46,55], and corresponds to the depth distributions of Au and Ag ions [56]. By careful analysis of the TEM micrographs, one observes dark-contrast areas predominantly present in the damaged region, where the degree of structural modification of the layers as well as the number of dark regions is increasing with increasing fluence of Ag ions. The observed image contrast originates from a high atomic mass and, consequently, reflects the presence of agglomerates/clusters of Au and Ag atoms [45]. This is supported by corresponding SAED patterns, which shows extra isolated spots with interplanar spacings of 0.236 nm, which fit well to the (111) crystal planes of Au and Ag [45], thus confirming the existence of metallic nanocrystals.

Next, we observed that the thermal treatment of the implanted samples resulted in the changes of the TiN lattice and partial recovering of the columnar films structure. Fig. 2 (a) displays high-magnification TEM image of the as-deposited TiN, whereas (b) and (c) show the layer implanted with Au and Ag ions to the fluence of 1×10^{16} ions/cm^2

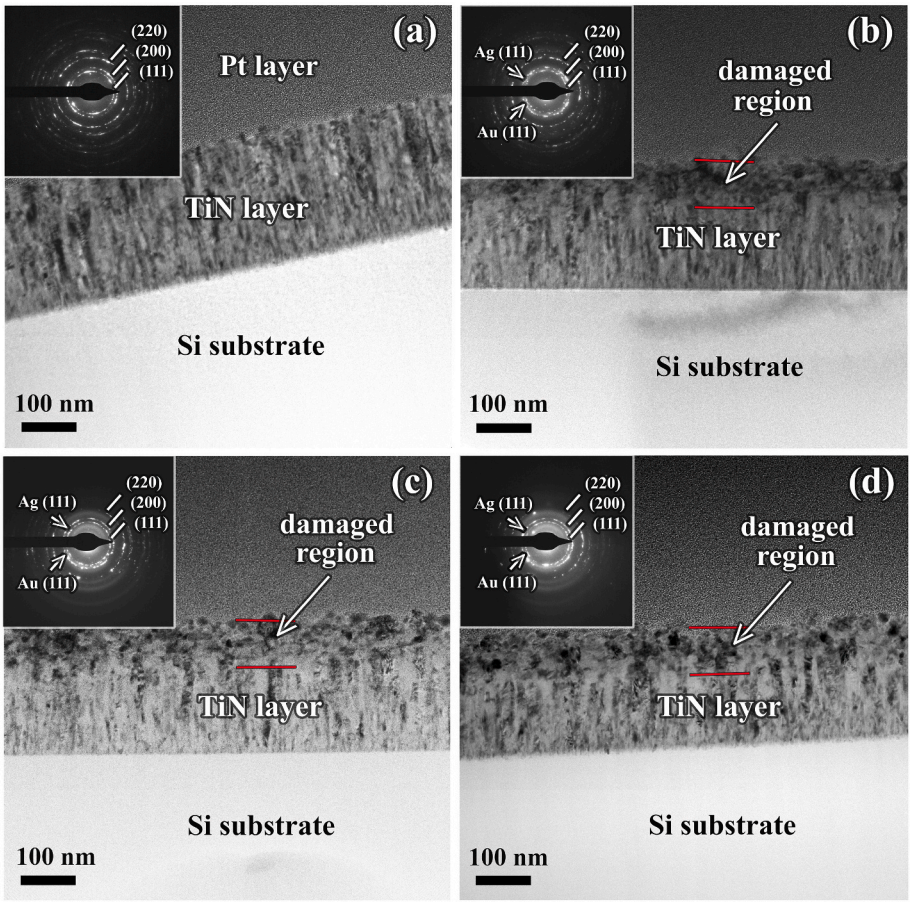

Fig. 1. Low magnification cross-sectional TEM bright-field micrograph of an as-deposited TiN thin film with a thickness of ~260 nm (a) and TiN films sequentially implanted with 1×10^{16} ions/cm^2 Au ions and 7×10^{16} ions/cm^2, 1×10^{17} ions/cm^2 and 13×10^{16} ions/cm^2 Ag ions (b, c and d, respectively), also presenting the Si substrates and Pt protective layers at the top of the samples (color lines represent depths of TiN layers where the most of the metal ions are stopped). Corresponding electron diffraction patterns taken from the selected area of the films are given in the insets.

and 7×10^{16} ions/cm^2, before and after annealing, respectively. By comparing the images, it is clearly observable that the structure affected by ion implantation was recovered after thermal treatment. In fact, this is expected since different diffusion mechanisms are promoted inside the layer during the annealing process, which lead to grain growth, annihilation of defects and overall to the formation of energetically more favorable structure [46]. Closer analysis of the microstructure was analyzed by HRTEM imaging, where the distances between two adjacent planes were measured. Based on the image of as-deposited layer, presented in Fig. 2 (d), it was found that the measured interplanar spacing of 0.244 nm correspond to (111) planes of TiN. Respective HRTEM micrographs of typical grains of implanted TiN, recorded before and after annealing, are displayed in Fig. 2 (e,f). As for the inter-spacing distance of (111) crystal planes for as-implanted sample we have measured the value of 0.243 nm, which is lower in comparison to the value of as-deposited film, thus indicating that the lattice is contracted after ion implantation. The change of the lattice parameter is even more pronounced after annealing, where the d-value was found to be 0.242 nm.

In addition to the TEM imaging, energy dispersive X-ray spectroscopy measurements of the samples were performed and an exemplary EDS spectrum of the TiN film implanted with 1×10^{16} ions/cm^2 of Au and 7×10^{16} ions/cm^2 of Ag is presented in Fig. 2 (g). The spectrum is characterized by Ti and N lines, but also exhibit peaks of Au and Ag, confirming the existence of the implanted metals. The presence of weak lines of oxygen and carbon in the spectra likely originate from O and C incorporation during the film growth, but also could be due to the exposure of TiN samples to atmospheric air. Besides, the EDS spectra were used for quantitative analysis characterization and the calculated composition of TiN samples is presented in Fig. 2 (h). It was found that the composition changes from almost stoichiometric TiN for the as-deposited film to $TiN_{0.96}$ for the sample implanted with Au and Ag ions to the highest ion fluence. Hence, the films become understoichiometric after implantation with deficient nitrogen content. A similar behavior was observed after annealing, although the effect was much pronounced in comparison to implanted samples, i.e. the composition deviates even more from the stoichiometric value.

The evolution of the crystal structure of the as-deposited, Au/Ag implanted and post-annealed TiN samples has also been studied by XRD and the measured diffraction patterns obtained for all samples are presented in Fig. 3. It can be seen that diffractogram of the as-deposited TiN film (Fig. 3a) exhibits two peaks at 36.19° and 42.13°, which could be assigned to the (111) and (200) planes (JCPDS #38–1420) of the face centered cubic TiN, respectively. After both ion implantation (b-d) and post-annealing (e-h) the diffractograms are not significantly changed in comparison to the as-deposited TiN. The crystallographic cubic structure is preserved; the primary phase of the films includes TiN (111) and TiN (200) reflections without the traces of any other phase, which clearly demonstrates that fcc TiN has a very high level of radiation hardness. However, the following observation can be made regarding the X-ray diffractograms of the treated samples: i) the shift of the diffraction maxima; ii) the reduction in the peak intensity, and iii) the broadening of the peaks. Firstly, it was found that for 4×10^{16} ions/cm^2 fluence of Ag ions the position of the (111) peak is significantly shifted toward higher 2θ angle from 36.19° to 36.54°, graph 3(d), indicating a decrease in the corresponding d-spacing and the reduction of TiN lattice. The lattice constant of the as-deposited TiN sample was determined by using the Le Bail's whole profile unit cell refinement [57] within FullProf program and found to be 0.4295 nm, which is in a good agreement with the values reported previously [24,58,59]. After implantation the lattice constant decreases to 0.4260 nm, which represents almost 1% contraction of unit cell size. With increasing silver ion fluence, the lattice

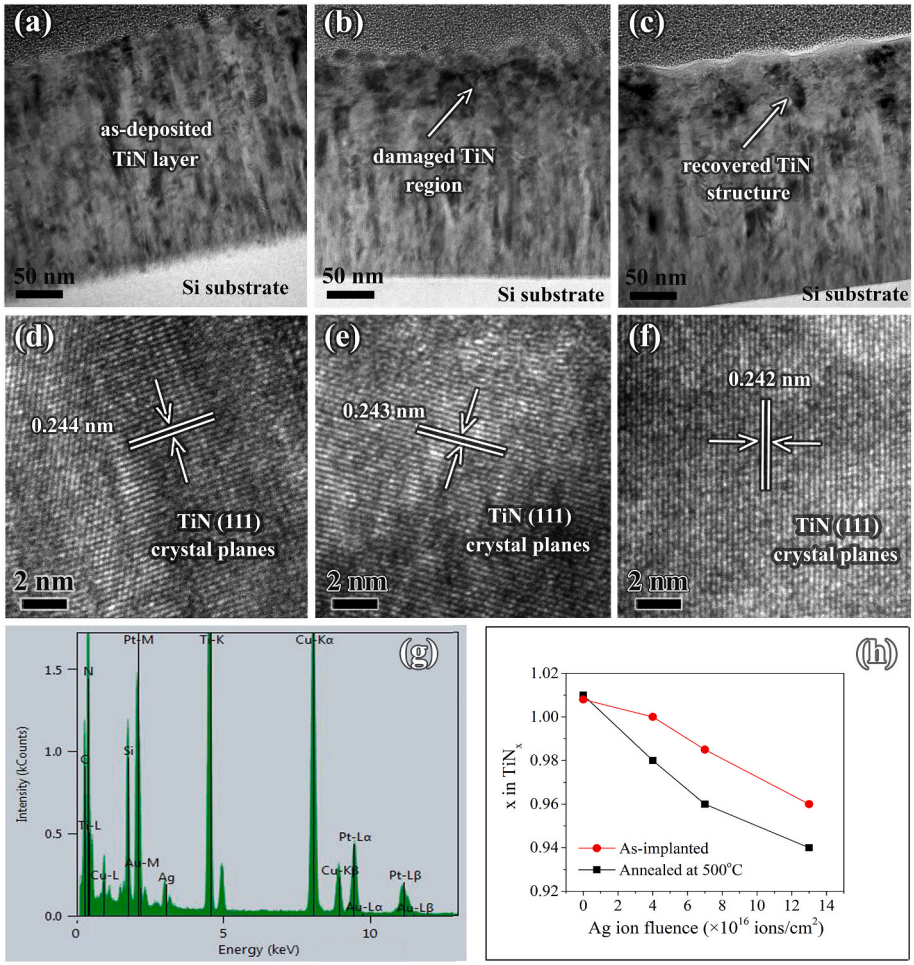

Fig. 2. High-magnification TEM micrographs (a,b,c) and respective HRTEM images (d,e,f) of the as-deposited TiN film and the layers sequentially implanted with 1×10^{16} ions/cm^2 Au ions and 7×10^{16} ions/cm^2 Ag ions, before and after annealing, respectively, with measured crystal plane spacings. An exemplary EDS spectrum taken from TiN film implanted with 1×10^{16} ions/cm^2 Au ions and 7×10^{16} ions/cm^2 Ag ions is shown in (g). The graph in (h) presents the variation of the composition of TiN films with silver ion fluence, as determined from EDS analysis (the values were estimated with an error of about 1 at.%).

constant decreases, as summarized in Fig. 4(a). The observed changes could be interpreted in the frame of stress-related effects and considerable damage induced by the presence of foreign ions in the films thus provoking additional stress in the lattice. Also, the decrease in lattice parameter could be related to the deficiency of nitrogen in agreement with literature [60]. The positions of both peaks are located at higher angles after the annealing treatment, as shown in graphs 3(e-h), in comparison with the as-implanted samples, meaning that the temperature additionally reduced the lattice parameter.

Besides, based on the changes in XRD diffraction patterns, i.e. from the broadening of the characteristic (111) and (200) reflections, we have calculated the grain size of the crystallites and also the induced micro-strain in the TiN films. The variation of crystallite size with increasing silver ion fluence is presented in Fig. 4(b). The Au/Ag sequential irradiation leads to a decrease in crystallite size from ~15 nm to ~10 nm, depending on the silver ion fluence which is in agreement with our previous studies related to modification of TiN using both metal and inert ion species [47,56]. The formation of smaller crystallites reflects a relatively high destabilizing effect of defects to the total free energy in crystals [46,61]. This could be combined with another mechanism who is also responsible for the formation of the small crystallites and coming from the short-range diffusion to grain boundaries [47,62]. The role of the temperature on the crystallite size was also investigated, where the crystallites become larger after annealing, with values between ~22 nm and ~15 nm depending on the Ag content, as also shown in Fig. 4(b). This trend is expected because the thermal treatment provides additional energy to the system allowing grains to merge together, which finally leads to the formation of the larger crystallites.

The variation of the micro-strain with increasing Ag ion fluence for the as-implanted and annealed TiN films is shown in Fig. 4(c). A micro-strain of 0.242% is observed for the as-deposited sample, which increases significantly after implantation reaching a value of 0.725% for the highest silver ion fluence. Since the micro-strain is related to the distortions of the structure, its increase could be assigned to the high concentration of irradiation induced defects and dislocations. This is in line with TEM characterization, which found that the metal ions irradiation strongly affects the structure of the film forming a high damage region in the zone where most of the ions are stopped [58]. Post-annealed samples show lower micro-strain compared to as-implanted ones, below 0.6%, due to the relaxation of the strain [59,60] and possible thermal activation of surface diffusion which starts at 500 °C. Finally, from XRD analysis it should be also mentioned that the observed intensity reduction of the (111) and (200) reflections is a result of the disruption of the TiN crystal structure, which happens during Au and Ag irradiation.

3.2. Optical properties of the films

In order to obtain detailed information on the optical properties of the implanted TiN films, the samples were analyzed using spectroscopic ellipsometry measurements. Fig. 5(a) shows the real part (ε_r) of the complex dielectric function of the as-deposited TiN thin film and films subsequently implanted with Au and varying Ag ion fluences. The ellipsometry data show that the as-deposited TiN film exhibits an optical transition at around 509.2 nm from dielectric to metallic behavior characterized by a positive to negative change in ε_r. The negative values originate from the interaction of light with the conduction electrons of TiN due to intraband (free-carrier) absorption representing the metallic

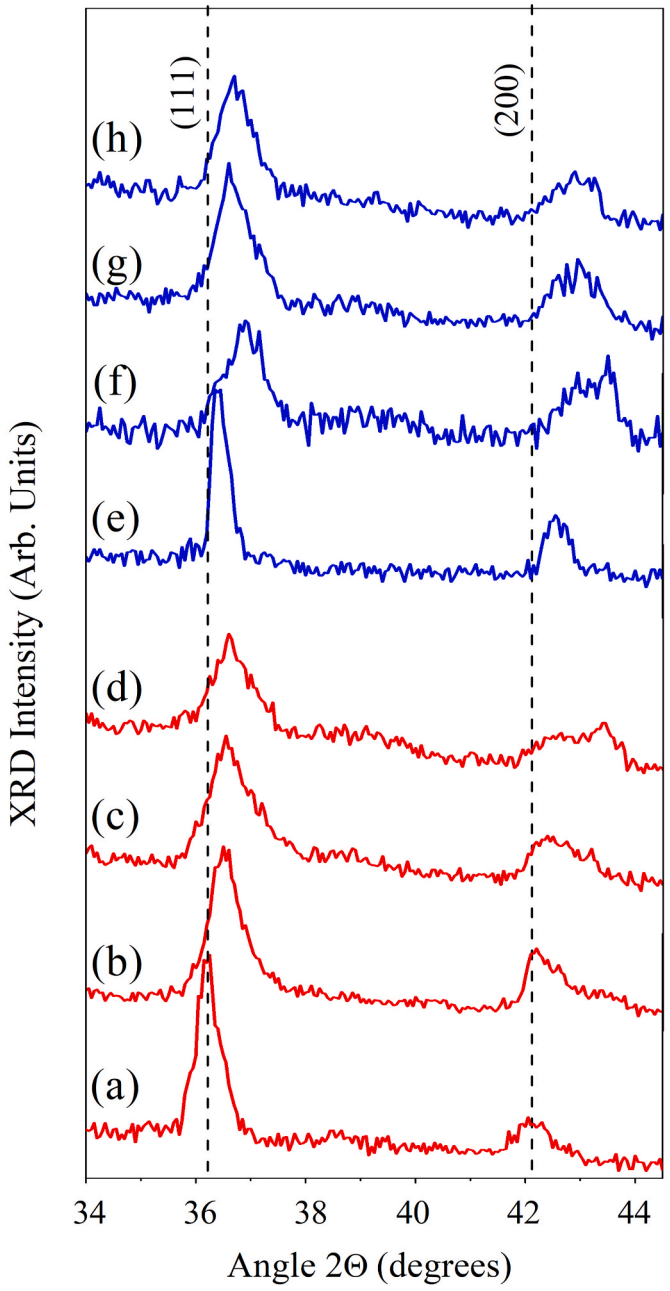

Fig. 3. XRD diffractograms of all samples. Red color represents spectra of as-deposited TiN (a) and the films sequentially implanted with Au ions to the fluence of 1×10^{16} ions/cm^2 and with silver ions to the different fluences of 4×10^{16} ions/cm^2, 7×10^{16} ions/cm^2 and 13×10^{16} ions/cm^2 (b,c and d, respectively). Blue color represents spectra of the samples taken after annealing at 500 °C (e–h).

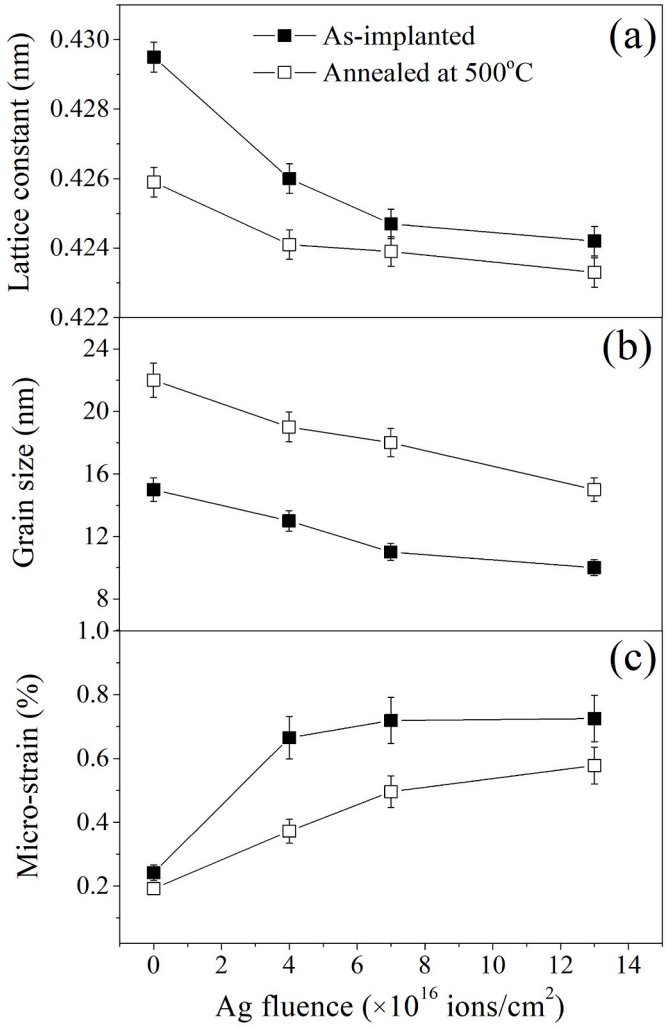

Fig. 4. Evolution of the lattice constant (a), grain size (b) and micro-strain (c) with increasing ion fluence of silver for as-implanted (closed symbols) and post-annealed (open symbols) TiN thin films at 500 °C. R_{wp} of the Le Bail's refinements ranged between 7.1% and 7.4%.

nature of TiN, while the presence of interband (bound-carrier) transitions makes ε_r slightly positive in the low wavelength range. The real part decreases monotonically with increasing wavelength due to the high electron concentration (around 10^{20}-10^{21} cm^{-3}) and exhibits a low value of about −50 at 2066 nm, which is well in agreement with the references [23,35,63]. Such a large negative ε_r value makes TiN useful in the area of plasmonics, thus being a good alternative material besides Au or Ag.

The real part of the dielectric function shows significant deviations after implantation, which are particularly evident in the near-IR spectral range ($\lambda > 900$ nm), where interband transitions are expected to be less important. The implanted films exhibit a lower negative ε_r, which is in contrast to the expectation that adding more noble metal atoms (Au and Ag) into a metal-like TiN matrix should lead to an even more metallic response. The decrease in metallicity could be attributed to the formation of implantation damage, such as the formation of point or extended defects but also surface sputtering, heavily affecting the surface morphology and the microstructure (e.g., changes in lattice constant, grain size as well as induced stress/strain as found by XRD). Nonetheless, changes in stoichiometry could also be responsible for the variation in optical response of TiN, in a way that the as-deposited sample, which is nearly stoichiometric, is characterized by the most negative value of ε_r. On the other hand, the less negative value of ε_r belongs to the TiN sample implanted with an Ag ion fluence of 13×10^{16} ions/cm^2, which is the most understoichiometric sample, but stays well below zero demonstrating that the implanted TiN thin films still exhibit a metallic response in the visible and near-IR range. Similar correlation between stoichiometry and magnitude of the real part of the dielectric function of TiN was found in the study of Judek et al. in Ref. [64], who investigated the plasmonic properties of nanocrystalline TiN films by changing its thicknesses and stoichiometry. In this sense, the variation in ε_r magnitude could be considered as a characteristic of the structural and chemical quality of TiN films [65]. The influence of annealing at 500 °C on the real part of the dielectric function is presented in Fig. 5(b). Although being more understoichiometric, the samples exhibit slightly

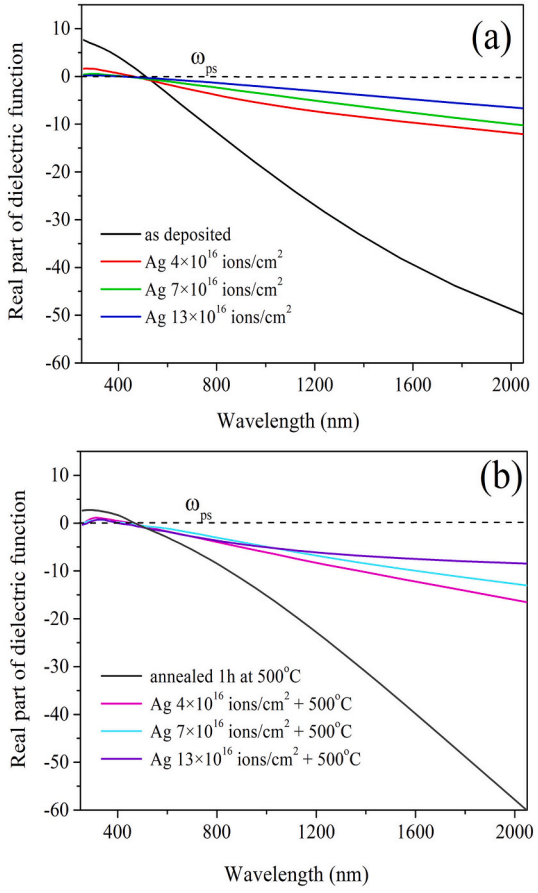

Fig. 5. The real part of the dielectric functions of as-deposited TiN thin film and after Au/Ag implantation (a) and post-annealing processing (b). In all samples the Au ion fluence was kept constant at 1×10^{16} ions/cm^2 while the silver ion fluence was varied (4×10^{16} ions/cm^2, 7×10^{16} ions/cm^2 and 13×10^{16} ions/cm^2); various colors correspond to different silver ion fluencies, as indicated in the legend.

larger ε_r values in comparison to the as-implanted situation. The more metallic behavior after annealing probably arises from recovering of the damaged structure after the high-temperature treatment, as already observed by TEM and presented in the text above.

To quantitatively explore the influence of the Au/Ag ion implantation and subsequent annealing on the dielectric function, we have analyzed the evolution of the screened plasma frequency (ω_{ps}), which is generally defined as the frequency at which the real part of the dielectric function crosses zero, signaling the onset of metallic behavior. It has been reported that the screened plasma frequency depends strongly on the composition of TiN, which can be used to monitor the stoichiometry of the films [65,66]. The value of 2.44 eV (wavelength 509.2 nm) obtained for the as-deposited sample is lower than the value of 2.6 eV for TiN_x ($x = 1$) reported by Adachi et al. in Ref. [67]. Nonetheless, this value is comparable to the results of Dimitriadis et al. [19], who determined that the ω_{ps} for TiN films falls between 2.36 eV and 2.68 eV for $1.04 \leq x \leq 0.99$. Our results show that the screened plasma frequency changes after implantation, as presented in Fig. 6, exhibiting a continuous increase with increasing silver ion fluence. We found that ω_{ps} increases from 2.44 eV (509.2 nm) to 3.03 eV (408.8 nm) for the highest silver ion fluence. The obtained shifting of the cross-section to higher energies (lower wavelengths) means that the ion implantation modifies the sample's composition. According to findings of Logothetidis presented in Ref. [68], the increase in plasma energy could be correlated with the nitrogen content in the implanted films, where the higher ω_{ps} values correspond to understiochiometric films with lower nitrogen

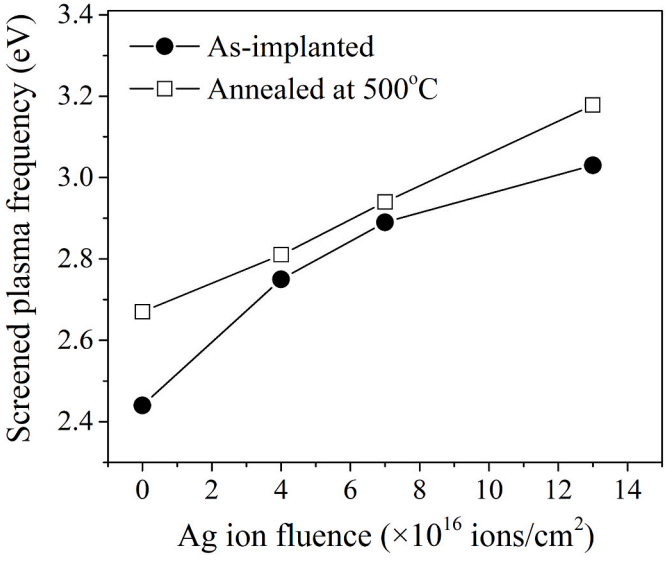

Fig. 6. The variation of screened plasma frequency as a function of the silver ion fluence of Au/Ag implanted (closed symbols) and post-annealed at 500 °C (open symbols) TiN thin films. The samples were implanted with Au ions to the fluence of 1×10^{16} ions/cm^2 and subsequently with silver ions to the different fluences of 4×10^{16} ions/cm^2, 7×10^{16} ions/cm^2 and 13×10^{16} ions/cm^2. The values of screened plasma frequency, which are taken from Fig. 5, are estimated with 1% of uncertainty.

concentration. Indeed, this fits to our TEM-EDS analysis presented above. This effect is more pronounced for the post-annealed samples and the values of the screened plasma frequency are higher in comparison to those obtained for the as-implanted situation. The correlation between the TiN composition and the screened plasma frequency is plotted in Fig. 7. It can be observed that ω_{ps} follows a linear relation with the nitrogen content in the film. Formally, the relation is: x (composition) = $0.0007 \cdot \omega_{ps}$ (nm) + 0.6648 for as-implanted films, Fig. 7(a). Similarly, the relation is: x (composition) = $0.0006 \cdot \omega_{ps}$ (nm) + 0.7092 for post-annealed samples, Fig. 7(b). These results fit well with the trends already reported in the literature [64,69,70].

To understand the changes in the optical properties of TiN film, it is necessary to get knowledge on the parameters that determine its dielectric function. The experimentally obtained spectroscopic ellipsometry data (Ψ, Δ) were analyzed using the optical model described in detail in our previous studies [44,47]. Briefly, considering that TiN shows a typical free electron-like behavior, its dielectric function was described by using a Drude-Lorentz dispersion formula [35,71,72]:

$$\varepsilon = \varepsilon_\infty - \frac{\omega_{pu}^2}{\omega^2 - i\Gamma_D\,\omega} + \sum_{j=1}^{2} \frac{f_j\,\omega_{0,j}^2}{\omega_{0,j}^2 - \omega^2 + i\gamma_j\omega} \qquad (1)$$

Here, two Lorenz oscillators used in fitting the ellipsometric spectra showed best match between experimentally data and fitted spectra, in agreement with literature [26,73]. The background constant ε_∞ is larger than unity, due to high-energy contributions referring to transitions, which are not taken into account by the Lorentz terms. The second term in equation (1) is characterized by the unscreened plasma frequency (ω_{pu}) and Drude damping parameter (Γ_D). The unscreened plasma frequency is defined via the free electron density N and the effective mass of electrons m^* through the relation: $\omega_{pu} = \sqrt{4\pi e^2 N/m^*}$ [74]. The parameters f_j, $\omega_{0,j}$ and γ_j present the strength, resonance frequency (energy position) and damping (broadening) of each Lorenz oscillator, respectively.

Summarized fitted parameters of all TiN samples are presented in Table 1. The observed dependence of ε_r given by the ion implantation and subsequent annealing procedure can be understood by the Drude

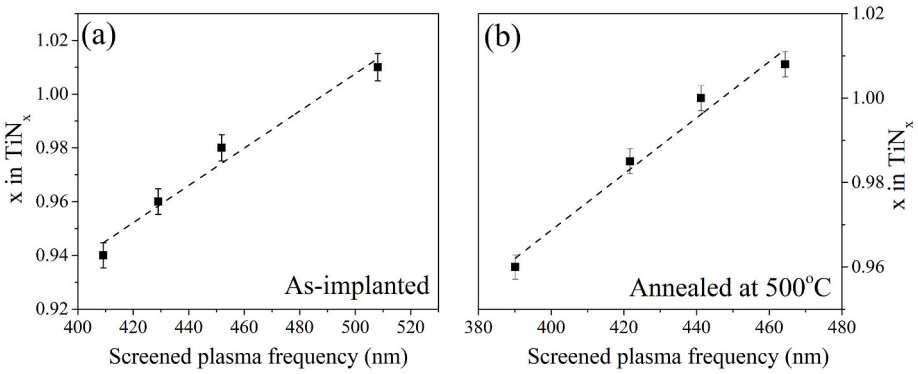

Fig. 7. Relation between the composition of the TiN samples (as measured from EDS analysis) and the screened plasma frequency (taken from Fig. 6 where ε_r equals zero).

Table 1
Fitted parameters of the Drude-Lorentz model of TiN films implanted with different Au/Ag fluences before and after annealing at 500 °C.

Sample treatment		Drude term			Lorentz term oscillator 1			Lorentz term oscillator 2		
		ε_∞	ω_{pu} (eV)	Γ_D (eV)	f_1	γ_1 (eV)	ω_{01} (eV)	f_2	γ_2 (eV)	ω_{02} (eV)
As deposited		1.06	5.35	0.53	2.05	13.01	5.02	3.60	7.43	6.41
1×10^{16} Au/cm^2	4×10^{16} Ag/cm^2	2.93	7.04	2.55	9.94	28.30	6.22	3.22	5.57	5.95
1×10^{16} Au/cm^2	7×10^{16} Ag/cm^2	2.55	10.42	4.60	28.35	48.50	6.90	3.06	3.88	5.73
1×10^{16} Au/cm^2	13×10^{16} Ag/cm^2	2.37	12.20	5.99	41.05	55.28	7.20	2.83	2.92	5.55
Annealed 1h at 500 °C		1.29	5.12	0.39	0.37	0.98	3.52	7.12	8.90	7.45
1×10^{16} Au/cm^2	4×10^{16} Ag/cm^2+500 °C	0.80	6.41	1.89	3.89	9.50	6.39	4.84	6.63	6.12
1×10^{16} Au/cm^2	7×10^{16} Ag/cm^2+500 °C	1.09	9.01	3.74	8.35	29.35	8.01	3.32	5.50	5.58
1×10^{16} Au/cm^2	13×10^{16} Ag/cm^2+500 °C	2.17	10.97	4.77	10.85	39.85	8.99	2.05	4.90	5.01

term in equation (1), i.e. by the parameters ω_{pu} and Γ_D. In Fig. 8 we present the variation of ω_{pu} (a) and Γ_D (b) with silver ion fluence, for as-implanted TiN samples as well as after annealing at 500 °C. Considering the parameters of the fits, we found that ω_{pu} changes after implantation, showing an increase of plasma energy from 5.35 eV for as-deposited sample to 12.20 eV for TiN film implanted to 1×10^{16} ions/cm^2 of Au and 13×10^{16} ions/cm^2 of Ag. In the case of the as-implanted samples, an increase in ω_{pu} is attributed to an increase of the carriers density due to the presence of Au and Ag atoms, which should lead to an enhancement of the metallic character of TiN. Such behavior is in contradiction with the decreasing trend of ε_r after implantation, which shows that the films become less metallic. This practically means that the decrease in the magnitude of ε_r is obviously not determined by the unscreened plasma frequency in this case, but is influenced by some other factors, as will be discussed below. The plasma frequency exhibits lower values after annealing in comparison to as-implanted films, probably due to reduction of the free electron density at higher temperature. Another factor in the Drude expression is the damping Γ_D, which is defined according to the free-electron theory as inverse of the electron relaxation time and it is directly correlated with the existence of grain boundaries, defects, phonons and electron-electron interactions [75]. After implantation, we found that Drude broadening becomes significantly larger, as shown in Fig. 8(b), approximately by one order of magnitude in the case of the highest Ag ion fluence, which we have expected due to large structural damage occurring upon ion irradiation. Indeed, according to the relation for the real part of dielectric function: $\varepsilon_r = -\omega_{pu}^2/\omega^2 + \Gamma_D^2$ [30], it is evident that the observed decrease in the magnitude of ε_r found for as-implanted samples is mainly given by the increase in Γ_D, while the contribution from ω_{pu} is marginal. The values of the Drude broadening are still significantly high after annealing, but overall lower in comparison with non-annealed samples due to the annihilation of defects at higher temperatures.

The parameters of the Lorentz oscillators (third term in eq. (1)) in TiN films also vary with the Ag ion fluence and post-annealing

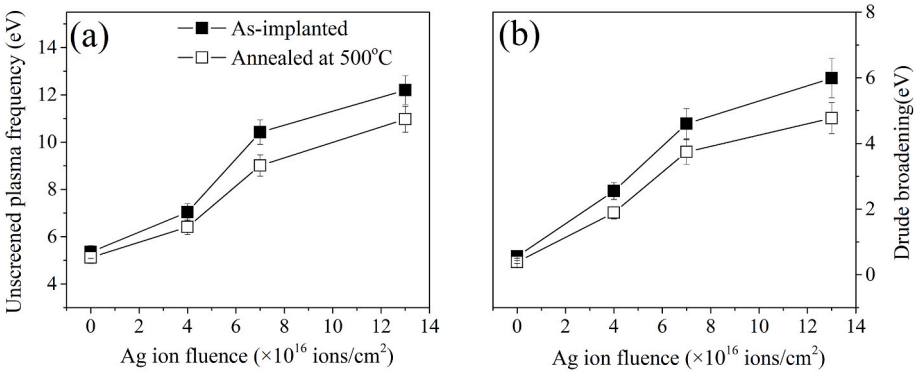

Fig. 8. The variation of unscreened plasma frequency (a) and Drude broadening (b) with silver ion fluence for TiN thin films sequentially implanted with 1×10^{16} ions/cm^2 of Au and different Ag ions fluences, before and after annealing at 500 °C.

treatment, as shown in Fig. 9. It can be seen that the increase in silver content shifts the ω_{01} oscillator frequency to higher energies from 5.02 eV to 7.20 eV, while ω_{02} decreases to lower energies from 6.41 eV to 5.55 eV. Further, after annealing at 500 °C the Lorentz frequency ω_{01} also increases from 3.52 eV to 8.99 eV and ω_{02} decreases from 7.45 eV to 5.01 eV. Here, it should be noted that this first Lorentz parameter mainly depends on the electronic structure of TiN and less to other factors, and any such modification should be due to stoichiometry and consequently to lattice parameter size [26]. The other two Lorentz parameters, broadening (γ_1) and strength (f_1), show a similar opposite trend for all processed samples, both implanted and post-annealed. The broadening and strength of the first oscillator increases while γ_2 and f_2 decrease with silver ion fluence. The origin of this behavior is difficult to explain due to complexity of these two Lorentz parameters especially the broadening that may be affected by the defects and crystallite size in addition to film stoichiometry [26].

Parallel to the real part of the dielectric function, ion implantation of silver and gold ions into TiN films as well as subsequent annealing also affects the imaginary part (ε_i), as shown in Fig. 10 (a,b). For comparison, referent ε_i values of the pure Ag and Au taken from Ref. [76] are also included in the figure. Characteristic feature of the spectra is a presence of a weak absorption band in the visible range, below 500 nm (see the inset in the figure) which originates from the surface plasmon resonance absorption of metal nanoparticles formed in the TiN film during the implantation processes [45,77]. After thermal annealing the SPR peak is more intense which comes from the formation of a larger number of nanoparticles and their subsequent growth. However, the most important information that can be obtained from the imaginary part of dielectric function is regarded to the optical losses of the material. Due to the interband transitions in the visible spectral range and due to the intraband transitions arising from free carrier contributions in the near-IR range, the optical losses of as-deposited TiN thin films are higher in comparison to pure Au and Ag. This restricts the use of TiN for practical applications in the area of plasmonics. However, after Au/Ag implantation the imaginary part significantly decreases indicating less absorptive films. The imaginary part at long wavelengths ($\lambda > 900$ nm) for the sample with the highest silver ion fluence becomes almost four times smaller in comparison to as-deposited TiN. From the stoichiometry point of view, it looks that the least lossy sample is the most understoichiometric film, which is the sample implanted to the highest Ag ion fluence. This practically means that the samples with the highest nitrogen deficiency possess lower losses than the stoichiometric as-deposited sample. The observed behavior in ε_i can be understood, similarly as in the case of ε_r, by noting that the increase in implanted metal ions increases the damage in the films making the Drude broadening larger. If we now have a closer look to the imaginary part of the dielectric function: $\varepsilon_i = \omega_{pu}^2 \Gamma_D / \omega(\omega^2 + \Gamma_D^2)$ [30], we can see that the magnitude of the imaginary part of ε is also determined by two parameters, ω_{pu} and Γ_D. In fact, one notices that the quadratic dependence of the denominator on Γ_D dominates and leads to a final decrease. After annealing at 500 °C, we observe that the magnitude of ε_i continues to decrease and becomes even lower than for Au and comparable to Ag. The possible reason for such behavior is when the annealing temperature is increased, the point defects were annealed out, the grain boundaries start to move and grains merge together forming larger crystals, which leads to an increase in the mean free path of the electrons and, hence, reduces ε_i. From the fitting results in Table 1, we can also see that both factors Γ_D and ω_{pu} are smaller after annealing, which means that the decreasing trend in ω_{pu} is obviously the dominant factor resulting into smaller values of ε_i.

4. Conclusions

In this work, we have investigated the effects of sequential Au/Ag ion

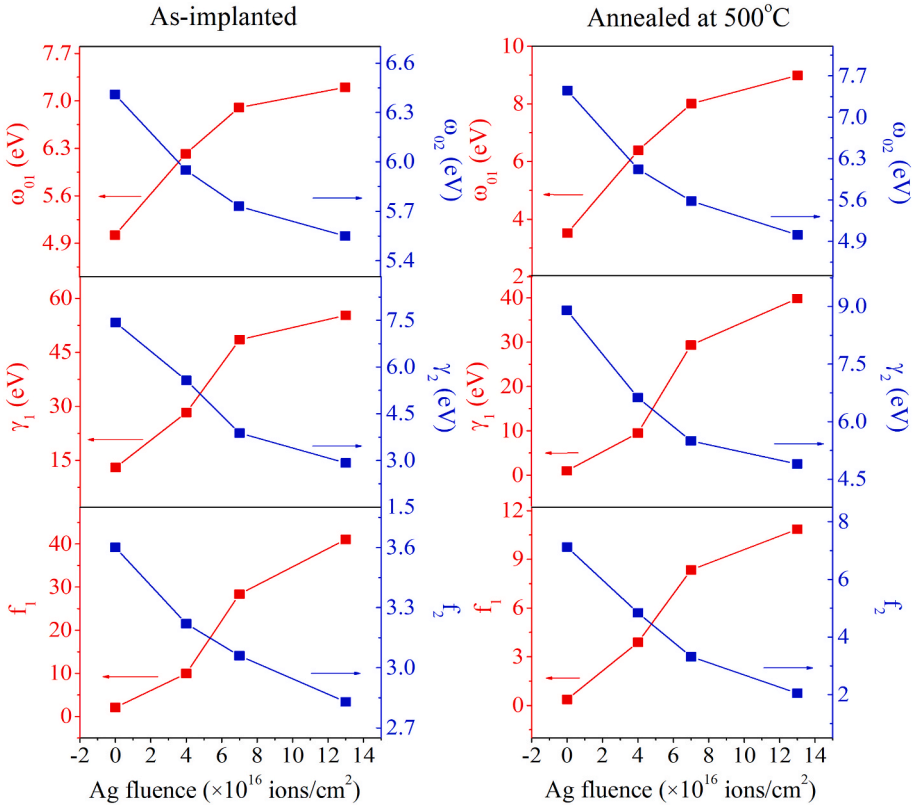

Fig. 9. The variation of the strength parameter, dumping factor (broadening parameter) and energy position of the Lorentz oscillators as a function of the Ag ion fluence for TiN thin films sequentially implanted with Au and Ag ions and after annealing at 500 °C. The films were firstly implanted with Au ions to the fluence of 1 × 10^{16} ions/cm^2 and then with different fluences of silver ions. Red and blue colors indicate the first and the second Lorentz oscillator, respectively.

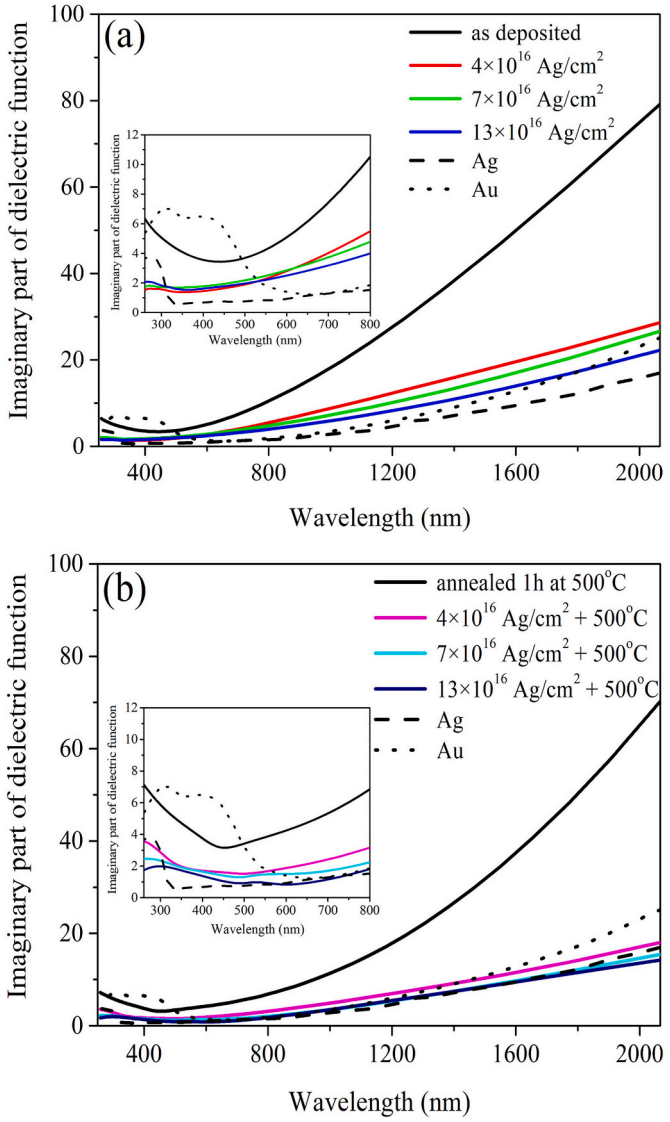

Fig. 10. The imaginary part of the dielectric functions of the as-deposited TiN thin film and after Au/Ag implantation (a) and post-annealing processing (b) with the insets which present enlarged spectral range between 260 nm and 800 nm, showing SPR peak coming from metal nanoparticles. In all samples the Au ion fluence was kept constant at 1×10^{16} ions/cm^2 while the silver ion fluence was varied (4×10^{16} ions/cm^2, 7×10^{16} ions/cm^2 and 13×10^{16} ions/cm^2); various colors correspond to different silver ion fluences as indicated in the legend. The imaginary parts of dielectric function for bulk Ag and Au are also included in graphs [76].

irradiation and subsequent annealing on the structural and optical properties of TiN thin films deposited by DC reactive sputtering on Si substrates. Our findings showed that the ion implantation destroyed the columnar structure of the films, forming Au and Ag metal nanoparticles in the near surface zone that also affects the TiN stoichiometry, lattice parameter and grain size. The implanted films become less stoichiometric with reduced lattice parameter and exhibit smaller TiN crystallites in comparison to the as-deposited layer. After annealing the damaged structure is partially recovered, the TiN crystallites become larger while the lattice size continues to decrease. In line with the modification of the structure of the films, the optical properties change, as seen by the variation of both the real and imaginary parts of the dielectric function. The implanted films exhibited overall less metallic character and the optical losses are significantly reduced in comparison to the initial TiN layer. After subsequent thermal treatment the films are better metals, but exhibit losses even lower than those of the as-implanted samples, being comparable to Au and Ag. The observed optical response of such treated TiN samples primarily comes from the variation in stoichiometry and different microstructural changes. This is visible through the variation of unscreened plasma frequency and Drude broadening. These findings showed that the optical quality of TiN films can be well controlled and improved by varying the metal ion fluences and post-processing annealing which could be especially useful in the area of plasmonics.

CRediT authorship contribution statement

M. Popović: Conceptualization, Investigation, Methodology, Validation, Formal analysis, Visualization, Writing – original draft, All authors have read and agreed to the published version of the manuscript. **M. Novaković:** Conceptualization, Investigation, Formal analysis, Writing – review & editing, All authors have read and agreed to the published version of the manuscript. **D. Vaňa:** Formal analysis, Software, All authors have read and agreed to the published version of the manuscript. **C. Ronning:** Resources, Writing – review & editing, All authors have read and agreed to the published version of the manuscript. **D. Jugović:** Resources, Investigation, Writing – review & editing, All authors have read and agreed to the published version of the manuscript. **V. Rajić:** Investigation, All authors have read and agreed to the published version of the manuscript. **P. Noga:** Resources, Investigation, Software, Writing – review & editing, All authors have read and agreed to the published version of the manuscript.

Declaration of competing interest

The authors declare that they have no known competing financial interests or personal relationships that could have appeared to influence the work reported in this paper.

Data availability

Data will be made available on request.

Acknowledgments

The work was supported by the Ministry of Education, Science and Technological Development of the Republic of Serbia (contract No. 451-03-9/2021-14/200017 and No. 451-03-9/2022-14/200017), the German-Serbian DAAD bilateral collaboration (Project No. 451-03-01971/2018-09/3), the Slovak Research and Development Agency (Project. No. APVV-18-0168) and the European Structural Development Funds (Project No. ITMS2014 + 313011W085). We thank Dr. Davor Peruško for his assistance with films deposition processes. The authors are (partly) members of the COST Action FIT4NANO CA19140 (http://www.fit4nano.eu/).

References

[1] W. Bi, Z. Hu, X. Li, C. Wu, J. Wu, Y. Wu, Y. Xie, Metallic mesocrystal nanosheets of vanadium nitride for high-performance all-solid-state pseudocapacitors, Nano Res. 8 (2015) 193–200, https://doi.org/10.1007/s12274-014-0612-y.
[2] B. Gao, X. Li, K. Ding, C. Huang, Q. Li, P.K. Chu, K. Huo, Recent progress in nanostructured transition metal nitrides for advanced electrochemical energy storage, J. Mater. Chem. A 7 (2019) 14–37, https://doi.org/10.1039/c8ta05760e.
[3] H.O. Pierson, Handbook of Refractory Carbides & Nitrides: Properties, Characteristics, Processing and Apps, William Andrew, 1996.
[4] J.K. Bal, S. Hazra, Interfacial role in room-temperature diffusion of Au into Si substrates, Phys. Rev. B 75 (2007), 205411, https://doi.org/10.1103/PhysRevB.75.205411.
[5] P. Patsalas, N. Kalfagiannis, S. Kassavetis, G. Abadias, D.V. Bellas, C. Lekka, E. Lidorikis, Conductive nitrides: growth principles, optical and electronic properties, and their perspectives in photonics and plasmonics, Mater. Sci. Eng. R 123 (2018) 1–55, https://doi.org/10.1016/j.mser.2017.11.001.

[6] H.E. Rebenne, D.G. Bhat, Review of CVD TiN coatings for wear-resistant applications: deposition processes, properties and performance, Surf. Coating. Technol. 63 (1994) 1–13, https://doi.org/10.1016/S0257-8972(05)80002-7.

[7] M. Nose, M. Zhou, E. Honbo, M. Yokota, S. Saji, Colorimetric properties of ZrN and TiN coatings prepared by DC reactive sputtering, Surf. Coating. Technol. 142–144 (2001) 211–217, https://doi.org/10.1016/S0257-8972(01)01196-3.

[8] N. Yokoyama, K. Hinode, Y. Homma, LPCVD titanium nitride for ULSIs, J. Electrochem. Soc. 138 (1991) 190–195, https://doi.org/10.1149/1.2085535.

[9] R.H. Dauskardt, M. Lane, Q. Ma, N. Krishna, Adhesion and debonding of multi-layer thin film structures, Eng. Fract. Mech. 61 (1998) 141–162, https://doi.org/10.1016/S0013-7944(98)00052-6.

[10] M.C. Lemme, J.K. Efavi, T. Mollenhauer, M. Schmidt, H.D.B. Gottlob, T. Wahlbrink, N. Kurz, Nanoscale TiN metal gate technology for CMOS integration, Microelectron. Eng. 83 (2006) 1551–1554, https://doi.org/10.1016/j.mee.2006.01.161.

[11] G.V. Naik, V.M. Shalaev, A. Boltasseva, Alternative plasmonic materials: beyond gold and silver, Adv. Mater. 25 (2013) 3264–3294, https://doi.org/10.1002/ADMA.201205076.

[12] K. Postava, M. Aoyama, T. Yamaguchi, Optical characterization of TiN/SiO_2 (1000 nm)/Si system by spectroscopic ellipsometry and reflectometry, Appl. Surf. Sci. 175–176 (2001) 270–275, https://doi.org/10.1016/S0169-4332(01)00095-2.

[13] H. Van Bui, A.Y. Kovalgin, R.A.M. Wolters, On the difference between optically and electrically determined resistivity of ultra-thin titanium nitride films, Appl. Surf. Sci. 269 (2013) 45–49, https://doi.org/10.1016/J.APSUSC.2012.09.074.

[14] W. Li, U. Guler, N. Kinsey, G.V. Naik, A. Boltasseva, J. Guan, V.M. Shalaev, A. V. Kildishev, Refractory plasmonics with titanium nitride: broadband metamaterial absorber, Adv. Mater. 26 (47) (2014) 7959–7965, https://doi.org/10.1002/adma.201401874.

[15] C.M. Zgrabik, E.L. Hu, Optimization of sputtered titanium nitride as a tunable metal for plasmonic applications, Opt. Mater. Express 5 (12) (2015) 2786–2797, https://doi.org/10.1364/OME.5.002786.

[16] Z.-Y. Yang, Y.-H. Chen, B.-H. Liao, K.-P. Chen, Room temperature fabrication of titanium nitride thin films as plasmonic materials by high-power impulse magnetron sputtering, Opt. Mater. Express 6 (2) (2016) 540–551, https://doi.org/10.1364/OME.6.000540.

[17] I.-S. Yu, H.-E. Cheng, C.-C. Chang, Y.-W. Lin, H.-T. Chen, Y.-C. Wang, Z.-P. Yang, Substrate-insensitive atomic layer deposition of plasmonic titanium nitride films, Opt. Mater. Express 7 (3) (2017) 777–784, https://doi.org/10.1364/OME.7.000777.

[18] B.W. Karr, I. Petrov, D.G. Cahill, J.E. Greene, Morphology of epitaxial TiN(001) grown by magnetron sputtering, Appl. Phys. Lett. 70 (13) (1997) 1703–1705, https://doi.org/10.1063/1.118675.

[19] C.A. Dimitriadis, J.I. Lee, P. Patsalas, S. Logothetidis, D.H. Tassis, J. Brini, G. Kamarinos, Characteristics of TiN_x/n-Si Schottky diodes deposited by reactive magnetron sputtering, J. Appl. Phys. 85 (1999) 4238–4242, https://doi.org/10.1063/1.370336.

[20] L. Hultman, H. Ljungcrantz, C. Hallin, E. Janzén, J.E. Sundgren, B. Pécz, L. R. Wallenberg, Growth and electronic properties of epitaxial TiN thin films on 3C-SiC(001) and 6H-SiC(0001) substrates by reactive magnetron sputtering, J. Mater. Res. 11 (1996) 2458–2462, https://doi.org/10.1557/JMR.1996.0309.

[21] K. Gammer, M. Stoiber, J. Wagner, H. Hutter, R. Kullmer, C. Mitterer, Investigations on the effects of plasma-assisted pre-treatment for plasma-assisted chemical vapour deposition TiN coatings on tool steel, Thin Solid Films 461 (2004) 277–281, https://doi.org/10.1016/J.TSF.2004.02.013.

[22] R.V. Babinova, V.V. Smirnov, A.S. Useenov, K.S. Kravchuk, E.V. Gladkikh, V. I. Shapovalov, I.L. Mylnikov, Mechanical properties of titanium nitride films obtained by reactively sputtering with hot target, J. Phys. Conf. 872 (2017), 012035, https://doi.org/10.1088/1742-6596/872/1/012035.

[23] K.C. Maurya, V.M. Shalaev, A. Boltasseva, B. Saha, Reduced optical losses in refractory plasmonic titanium nitride thin films deposited with molecular beam epitaxy, Opt. Mater. Express 10 (2020) 2679–2692, https://doi.org/10.1364/OME.405259.

[24] R. Manaila, F. Zavaliche, A. Devenyi, D. Biro, P.B. Barna, M. Adamik, S. Craciun, Ti nitride phases in thin films deposited by DC magnetron sputtering, Appl. Surf. Sci. 91 (1995) 295–302, https://doi.org/10.1016/0169-4332(95)00134-4.

[25] B. Karlsson, R.P. Shimshock, B.O. Seraphin, J.C. Haygarth, Optical properties of CVD-coated TiN, ZrN and HfN, Sol. Energy Mater. 7 (1983) 401–411, https://doi.org/10.1016/0165-1633(83)90013-8.

[26] P. Patsalas, S. Logothetidis, Optical, electronic, and transport properties of nanocrystalline titanium nitride thin films, J. Appl. Phys. 90 (2001) 4725–4734, https://doi.org/10.1063/1.1403677.

[27] P. Patsalas, C. Charitidis, S. Logothetidis, The effect of substrate temperature and biasing on the mechanical properties and structure of sputtered titanium nitride thin films, Surf. Coating. Technol. 125 (2000) 335–340, https://doi.org/10.1016/S0257-8972(99)00606-4.

[28] H. Liang, J. Xu, D. Zhou, X. Sun, S. Chu, Y. Bai, Thickness dependent microstructural and electrical properties of TiN thin films prepared by DC reactive magnetron sputtering, Ceram. Int. 42 (2) (2016) 2642–2647, https://doi.org/10.1016/j.ceramint.2015.10.070.

[29] F. Magnus, A.S. Ingason, O. Sveinsson, S. Olafsson, J. Gudmundsson, Room temperature fabrication of titanium nitride thin films as plasmonic materials by high-power impulse magnetron sputtering, Opt. Mater. Express 6 (2016) 540–551, https://doi.org/10.1364/OME.6.000540.

[30] H. Reddy, U. Guler, Z. Kudyshev, A.V. Kildishev, V.M. Shalaev, A. Boltasseva, Temperature-Dependent optical properties of plasmonic titanium nitride thin films, ACS Photonics 4 (2017) 1413–1420, https://doi.org/10.1021/acsphotonics.7b00127.

[31] U. Guler, S. Suslov, A.V. Kildishev, A. Boltasseva, V.M. Shalaev, Colloidal plasmonic titanium nitride nanoparticles: properties and applications, Nanophotonics 4 (2015) 269–276, https://doi.org/10.1515/nanoph-2015-0017.

[32] A. Capretti, Y. Wang, N. Engheta, L.D. Negro, Comparative study of second-harmonic generation from epsilon-near-zero indium tin oxide and titanium nitride nanolayers excited in the near-infrared spectral rrange, ACS Photonics 2 (11) (2015) 1584–1591, https://doi.org/10.1021/acsphotonics.5b00355.

[33] D. Shah, A. Catellani, H. Reddy, N. Kinsey, V.M. Shalaev, A. Boltasseva, A. Calzolari, Controlling the plasmonic properties of ultrathin TiN films at the atomic level, ACS Photonics 5 (2018) 2816–2824, https://doi.org/10.1021/acsphotonics.7b01553.

[34] C.M. Zgrabik, E.L. Hu, Optimization of sputtered titanium nitride as a tunable metal for plasmonic applications, Opt. Mater. Express 5 (12) (2015) 2786–2797, https://doi.org/10.1364/OME.5.002786.

[35] P. Patsalas, N. Kalfagiannis, S. Kassavetis, Optical properties and plasmonic performance of titanium nitride, Materials 8 (2015) 3128–3154, https://doi.org/10.3390/ma8063128.

[36] P.D. Townsend, P.J. Chandler, L. Zhang, Optical Effects of Ion Implantation, Cambridge University Press, 1994.

[37] A.L. Stepanov, Nonlinear optical properties of implanted metal nanoparticles in various transparent matrixes: a review, Rev. Adv. Mater. Sci. 27 (2) (2011) 115–145.

[38] E.N. Epie, D. Scott, W.K. Chu, Manipulating the optical properties of dual implanted Au and Zn nanoparticles in sapphire, Photon. Nanostruct: Fundam. Appl. 27 (2017) 17–23, https://doi.org/10.1016/j.photonics.2017.09.002.

[39] F. Ren, X.H. Xiao, G.X. Cai, J.B. Wang, C.Z. Jiang, Engineering embedded metal nanoparticles with ion beam technology, Appl. Phys. Mater. Sci. Process 96 (2009) 317–325, https://doi.org/10.1007/s00339-009-5205-3.

[40] Y.-Y. Chang, D.-Y. Wang, W. Wu, Tribological enhancement of CrN coatings by niobium and carbon ion implantation, Surf. Coating. Technol. 177-178 (2004) 441–446, https://doi.org/10.1016/S0257-8972(03)01030-2.

[41] K. Ibrahim, M. Mahbubur Rahman, H. Taha, E. Mohammadpour, Z. Zhou, C.-Y. Yin, A. Nikoloski, Z.-T. Jiang, Structural, morphological, and optical characterizations of Mo, CrN and Mo:CrN sputtered coatings for potential solar selective applications, Appl. Surf. Sci. 440 (2018) 1001–1010, https://doi.org/10.1016/j.apsusc.2018.01.267.

[42] Y.-U. Heo, M. Takeguchi, K. Mitsuishi, M. Song, Y. Nakayama, K. Furuya, Precipitation behavior of Xe at grain boundaries in Si_3N_4 ceramic during implantation at elevated temperature, J. Nucl. Mater. 397 (2010) 122–127, https://doi.org/10.1016/j.jnucmat.2009.12.018.

[43] M. Novaković, M. Popović, E. Schmidt, M. Mitrić, N. Bibić, Z. Rakočević, C. Ronning, Clustering of gold particles in Au implanted CrN thin films: the effect on the SPR peak position, Appl. Surf. Sci. 426 (2017) 667–673, https://doi.org/10.1016/j.apsusc.2017.07.233.

[44] M. Popović, M. Novaković, M. Mitrić, K. Zhang, Z. Rakočević, N. Bibić, Xenon implantation effects on the structural and optical properties of reactively sputtered titanium nitride thin films, Mater. Res. Bull. 91 (2017) 36–41, https://doi.org/10.1016/j.materresbull.2017.03.031.

[45] M. Popović, M. Novaković, P. Noga, D. Vaňa, Z. Rakočević, Synthesis of AuAg@Ag core/shell bimetallic nanoparticles in titanium nitride thin films by sequential ion implantation, Appl. Surf. Sci. 481 (2019) 1418–1424, https://doi.org/10.1016/j.apsusc.2019.03.243.

[46] M. Popović, M. Novaković, N. Bibić, Structural characterization of TiN coatings on Si substrates irradiated with Ar ions, Mater. Char. 60 (2009) 1463–1470, https://doi.org/10.1016/j.matchar.2009.07.002.

[47] M. Popović, M. Novaković, M. Mitrić, K. Zhang, N. Bibić, Structural, optical and electrical properties of argon implanted TiN thin films, Int. J. Refract. Metals Hard Mater. 48 (2015) 318–323, https://doi.org/10.1016/j.ijrmhm.2014.09.026.

[48] M. Novaković, M. Popović, P. Noga, D. Vaňa, C. Ronning, Low optical losses in plasmonic TiN thin films implanted with silver and gold, Opt. Mater. 123 (2022), 111936, https://doi.org/10.1016/j.optmat.2021.111936.

[49] M. Novaković, M. Popović, Investigating the optical response of titanium-nitride thin films after silver ion implantation and post-thermal annealing, Opt. Mater. 133 (2022), 112955, https://doi.org/10.1016/j.optmat.2022.112955.

[50] M. Popović, M. Novaković, A. Traverse, K. Zhang, N. Bibić, H. Hofsäss, K.P. Lieb, Modifications of reactively sputtered titanium nitride films by argon and vanadium ion implantation: microstructural and opto-electric properties, Thin Solid Films 531 (2013) 189–196, https://doi.org/10.1016/J.TSF.2013.01.045.

[51] P. Noga, J. Dobrovodský, D. Vaňa, M. Beňo, A. Závacká, M. Muška, R. Halgaš, S. Minárik, R. Riedlmajer, A new ion-beam laboratory for materials research at the Slovak university of technology, Nucl. Instrum. Methods Phys. Res. Sect. B Beam Interact. Mater. Atoms 409 (2017) 264–267, https://doi.org/10.1016/J.NIMB.2017.04.051.

[52] J.F. Ziegler, J.P. Biersack, U. Littmark, The Stopping and Ranges of Ions in Matter, New York, 1985. code SRIM2010, http://www.srim.org.

[53] R.W. Cheary, A. Coelho, A fundamental parameters approach to X-ray line-profile fitting, J. Appl. Crystallogr. 25 (1992) 109–121, https://doi.org/10.1107/S0021889891010804.

[54] Horiba Scientific, DeltaPsi2 Software, Reference Manual, NP/DeltaPsi2R.Fm/264202- 06/01/2010. Part Number: 31 087 091.

[55] M. Popović, M. Novaković, N. Bibić, Annealing effects on the properties of TiN thin films, Process. Appl. Ceram. 9 (2) (2015) 67–71, https://doi.org/10.2298/PAC1502067P.

[56] M. Popović, M. Novaković, P. Noga, D. Vaňa, Z. Rakočević, Ion beam synthesis of Au-Ag alloy nanoparticles in TiN thin films, Nucl. Instrum. Methods Phys. Res. Sect. B Beam Interact. Mater. Atoms 475 (2020) 20–27, https://doi.org/10.1016/J.NIMB.2020.04.032.
[57] A. LeBail, Whole powder pattern decomposition methods and applications: a retrospection, Powder Diffr. 20 (4) (2005) 316–326, https://doi.org/10.1154/1.2135315.
[58] J.E. Sundgren, Structure and properties of TiN coatings, Thin Solid Films 128 (1985) 21–44, https://doi.org/10.1016/0040-6090(85)90333-5.
[59] L.E. Toth, Transition Metal Carbides and Nitrides, Academic Press, New York, 1971.
[60] S. Nagakura, T. Kusunoki, F. Kakimoto, Y. Hirotsu, Lattice parameter of the non-stoichiometric compound TiN_x, J. Appl. Crystallogr. 8 (1) (1975) 65–66, https://doi.org/10.1107/S0021889875009545.
[61] P. Karvankova, M.G.J. Veprek-Heijman, D. Azinovic, S. Veprek, Properties of superhard nc-TiN/a-BN and nc-TiN/a-BN/a-TiB_2 nanocomposite coatings prepared by plasma induced chemical vapor deposition, Surf. Coating. Technol. 200 (2006) 2978–2989, https://doi.org/10.1016/J.SURFCOAT.2005.01.003.
[62] H. Wang, R. Araujo, J.G. Swadener, Y.Q. Wang, X. Zhang, E.G. Fu, T. Cagin, Ion irradiation effects in nanocrystalline TiN coatings, Nucl. Instrum. Methods Phys. Res. Sect. B Beam Interact. Mater. Atoms 261 (2007) 1162–1166, https://doi.org/10.1016/J.NIMB.2007.04.248.
[63] A. Catellani, A. Calzolari, Plasmonic properties of refractory titanium nitride, Phys. Rev. B 95 (2017), 115145, https://doi.org/10.1103/PhysRevB.95.115145.
[64] J. Judek, P. Wróbel, P.P. Michałowski, M. Ozga, B. Witkowski, A. Seweryn, M. Struzik, C. Jastrzebski, K. Zberecki, Titanium nitride as a plasmonic material from near-ultraviolet to very-long-wavelength infrared range, Materials 14 (22) (2021) 7095, https://doi.org/10.3390/ma14227095.
[65] S. Logothetidis, I. Alexandrou, A. Papadopoulos, In situ spectroscopic ellipsometry to monitor the process of TiNx thin films deposited by reactive sputtering, J. Appl. Phys. 77 (1998) 1043–1047, https://doi.org/10.1063/1.358963.
[66] S. Logothetidis, E.I. Meletis, G. Kourouklis, New approach in the monitoring and characterization of titanium nitride thin films, J. Mater. Res. 14 (1999) 436–441, https://doi.org/10.1557/JMR.1999.0062.
[67] S. Adachi, M. Takahashi, Optical properties of TiN films deposited by direct current reactive sputtering, J. Appl. Phys. 87 (2000) 1264–1269, https://doi.org/10.1063/1.372006.
[68] S. Logothetidis, A. Barborica, In-situ and real time room temperature oxidation studies of fcc TiN thin films, Microelectron. Eng. 33 (1997) 309–316, https://doi.org/10.1016/S0167-9317(96)00059-7.
[69] A. Bendavid, P.J. Martin, R.P. Netterfield, T.J. Kinder, Characterization of the optical properties and composition of TiN_x thin films by spectroscopic ellipsometry and X-ray photoelectron spectroscopy, Surf. Interface Anal. 24 (1996) 627–633, https://doi.org/10.1002/(SICI)1096-9918(19960916)24:9<627::AID-SIA149>3.0.CO;2-R.
[70] C.G.H. Walker, J.A.D. Matthew, C.A. Anderson, N.M.D. Brown, An estimate of the electron effective mass in titanium nitride using UPS and EELS, Surf. Sci. 412–413 (1998) 405–414, https://doi.org/10.1016/S0039-6028(98)00459-2.
[71] F. Wooten, Optical Properties of Solids, Academic, New York, 1972.
[72] N.W. Ashcroft, N.D. Mermin, Solid State Physics, Saunders College, Orlando, 1976.
[73] P. Patsalas, S. Logothetidis, Interface properties and structural evolution of TiN/Si and TiN/GaN heterostructures, J. Appl. Phys. 93 (2002) 989–998, https://doi.org/10.1063/1.1531812.
[74] R.M.A. Azzam, N.M. Bashara, Ellipsometry and Polarized Light, North-Holland, Amsterdam, 1977.
[75] H. Savaloni, A.R. Khakpour, Substrate temperature dependence on the optical properties of Cu and Ag thin films, Eur. Phys. J. Appl. Phys. 31 (2005) 101–112, https://doi.org/10.1051/epjap:2005053.
[76] E.D. Palik, Handbook of Optical Constants of Solids, Academic Press, London, 1998.
[77] M. Popović, M. Novaković, Z. Rakočević, N. Bibić, Tailoring the structural and optical properties of TiN thin films by Ag ion implantation, Nucl. Instrum. Methods Phys. Res. Sect. B Beam Interact. Mater. Atoms 389–390 (2016) 33–39, https://doi.org/10.1016/j.nimb.2016.11.013.